ISSN: 3067-2384
Research Article

World Journal of Sensors Network Research

Analysis of Non-Newtonian Lubricant Flow in Textured Hydrodynamic Plain Bearings: Comparison with Untextured Surfaces

Khellafi Ikram*, Bendaoud Nadia & Mehala Kadda

Lab of Carburants Gazeux and Environment, University of science and technology of Oran Mohamed-Boudiaf USTOMB;El Mnaouar, BP 1505, Bir El Djir 31000, Oran, Algeria

***Corresponding author:** Khellafi Ikram, Lab of Carburants Gazeux and Environment, University of science and technology of Oran Mohamed-Boudiaf USTOMB;El Mnaouar, BP 1505, Bir El Djir 31000, Oran, Algeria.

Submitted: 16 October 2025 **Accepted:** 23 October 2025 **Published:** 20 November 2025

https://doi.org/10.63620/MKWJSNR.2025.1045

Citation: *Khellafi, I., Bendaoud, N., Mehala, K. (2025). Analysis of Non-Newtonian Lubricant Flow in Textured Hydrodynamic Plain Bearings: Comparison with Untextured Surfaces. Wor Jour of Sens Net Res, 2(6), 01-14.*

Abstract

The performance of hydrodynamic plain bearings is strongly influenced by the rheological behavior of the lubricant and the surface texture of the bearing. In recent years, numerous studies have investigated the complex fluid–structure interactions involving rotors, bearings, supports, and lubricating media in rotating machinery such as turbines and electric motors. These interactions become even more intricate when non-Newtonian lubricants are considered, due to their viscosity dependence on shear rate and temperature. In this work, a comprehensive parametric numerical investigation is conducted to analyze the behavior of a non-Newtonian lubricant within a hydrodynamic plain bearing featuring a textured surface. The numerical simulations are performed using the CFD computational fluid dynamics (CFD) software. The governing equations, based on the Navier–Stokes and continuity formulations, are solved to evaluate the influence of texture geometry, lubricant rheology, and operating conditions on the hydrodynamic pressure distribution and load-carrying capacity. The results demonstrate that surface texturing significantly enhances the hydrodynamic pressure and improves lubrication performance when compared to a smooth bearing. Furthermore, the non-Newtonian nature of the lubricant leads to an overestimation of pressure peaks and a more uniform film thickness distribution, contributing to improved bearing stability and reduced frictional losses. These findings highlight the combined benefits of surface texturing and non-Newtonian fluid behavior for optimizing the design of high-performance hydrodynamic bearings used in advanced rotating systems.

Keywords: Textured Hydrodynamic Plain Bearing, Non-newtonian Fluid, Tribological Behavior, Newtonian Fluid, Hydrodynamic Characteristics, and Pressure.

Introduction

Rotating machines occupy a preponderant place in industry and have a very varied use. In machines, hydrodynamic bearings are tribological components that support a load and guide transmission shafts in rotation. Non-Newtonian fluids, on the other hand, see their viscositychange under the effect of mechanical stress. They become either more viscous or more fluid when tapped, shaken or stirred. Non-Newtonian effects can be of two types: shear thinning effects and viscoelastic effects. Shear thinning effects, often called non- Newtonian effects. A fluid is said to be Newtonian when its viscosity is independent of the mechanical stress applied to it.

In 1990, Gecim published a work on shear thinning effects. It shows some examples and technical solutions for the treatment of non- Newtonian effects in plain bearings. It presented a new constitutive law, based on the right cross. The advantage of this law is that it has only one parameter to adjust (the stability coefficient).

In 1998, Zhang and colleagues analyzed the combined effects of roughness, shear thinning, and purely longitudinal, transverse, and isotropic viscoelasticity of engine oils on dynamically loaded finished plain bearings under mixed lubrication, using the Christensen stochastic model for hydrodynamic lubrication

of rough surfaces and considering the operating effect on the roughness height distribution. Shear thinning and viscoelasticity are characterized by the power law and Maxwell fluid models, respectively.

The results show that the combined effect of roughness and non-Newtonian rheology on bearing characteristics is closely related to the texture and structure of the roughness, the characteristics of the nominal geometry, the journal mass, and the operating conditions.

In 2000, Zhang and Cheng conducted a transient non-Newtonian thermohydrodynamic (THD) analysis of dynamically loaded journal bearings under mixed lubrication. Mass-conserving cavitation is included, and shear thinning and viscoelasticity are characterized by the power-law and upper-convection Maxwell models, respectively. The 2D energy equation is solved-with ISOADI (isothermal shaft and adiabatic inner ring surface) boundary conditions. The bearing is treated as a quasi-steady thermal element.

In 2001 and 2002, Wang et al. presented a numerical study on the effects of non-Newtonian lubricant behavior for elliptical-shaped plain bearings subjected to transient loads. The analysis is based on the mass-conserving finite element cavitation model. The results reveal that non- Newtonian effects have a significant influence on the bearing operating performance. They also addressed the influence of shear thinning effects in dynamic bearings, while taking into account the non-Newtonian behavior and the effect of rough surface geometry as well as the elliptical shape of the vane. They show that there is a significant increase in the maximum film pressure and flow rate while a significant reduction in the minimum film thickness and dissipation power. Kane in 2003 shows the effect of roughness and non-Newtonian effects in severe contact lubricants such as bearings. He presented a new modified Reynolds equation called non-Newtonian, using rheological laws and the basics of continuum mechanics applied to thin layers. The resolution of this equation gives the influential parameters on the geometry and rheology; these results have been validated with non-Newtonian theory.

In 2005 Fatu presents a numerical and experimental modeling of the lubrication of motor bearings subjected to severe operating conditions with the laws of variation of the appropriate viscosity, it can highlight the respective influence of non-Newtonian and piezoviscous effects in the complex case of large end bearings. Fatu showed that the piezoviscous effect turns out to be the most significant effect on the behavior of the bearing.

Additionally, since polymer-containing oils are expected to have a decrease in viscosity and normal stresses at high shear rate, thus having non- Newtonian behavior, the rheological properties were examined as a function of operating condition levels by Moritsugu KASAI in 2010. The results show temperature and pressure in the supposed non-Newtonian fluid film are high, with a coefficient n greater than 1, that is to say for viscoelastic fluids. In 2016 Javorova and colleagues presented a study of a hydrodynamic bearing examining flexible deformation and non-Newtonian fluids, using the Rabinowitsch fluid model. They showed that higher values of membrane pressure and load capacity were obtained on dilute lubricants, while false lubricants and oil film pressure were less significant.

Mehala and his collaborators presented in 2016 a study on the impact of the behavior of a non- Newtonian fluid for plain bearings working under severe operating conditions. The non-Newtonian behavior of lubricants (oils containing PM3 polymers) was analyzed numerically, the effect of temperature in laminar regime is also introduced, by solving the energy equation by the finite difference method.

The Non-Newtonian Fluids

There are 5 types of non-Newtonian fluids.

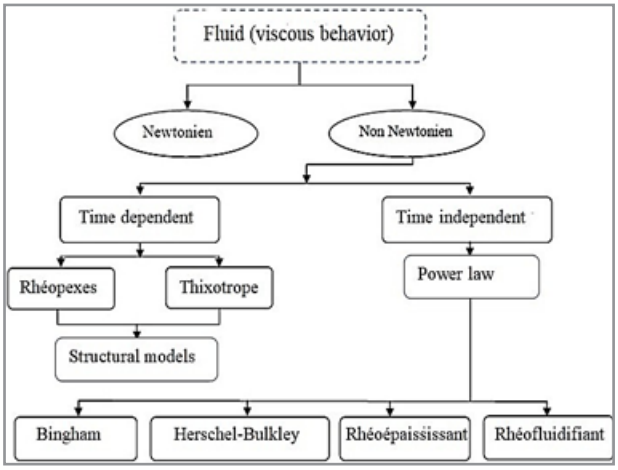

Figure 1: Classification of rheological behaviors.

Non-Newtonian fluid with time-independent behavior

These are fluids whose effective viscosity does not decrease with time when we apply a constraint on their behavior. Structural changes occurring in the fluid over time.

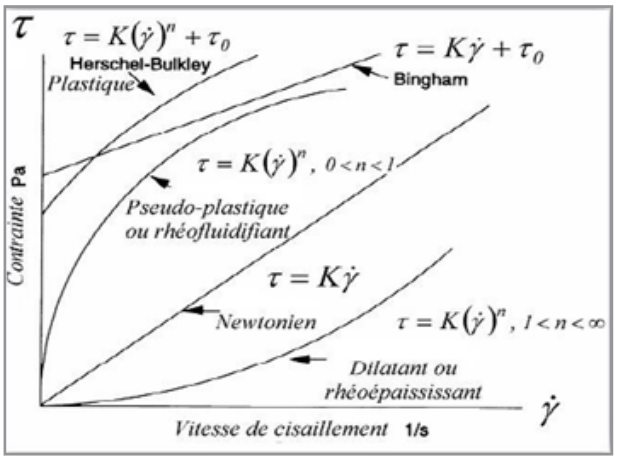

Figure 2: Rheogram of some categories of fluids.

Non-Newtonian Fluid with Behavior Dependent on Time

There are also fluids influenced by duration, these are thixotropic fluids and anti-thixotropic fluids.

Hydrodynamic Bearnings

The hydrodynamic bearings are frequently used, the simplest are made up of two elements, a cylindrical shaft generally made of steel of radius Ra which rotates inside a bore, (Figure 3) and the bearing made of bronze or regulated steel of radius interior in steel Rc and length L the characteristics of our bearing are indicated in figure 4.

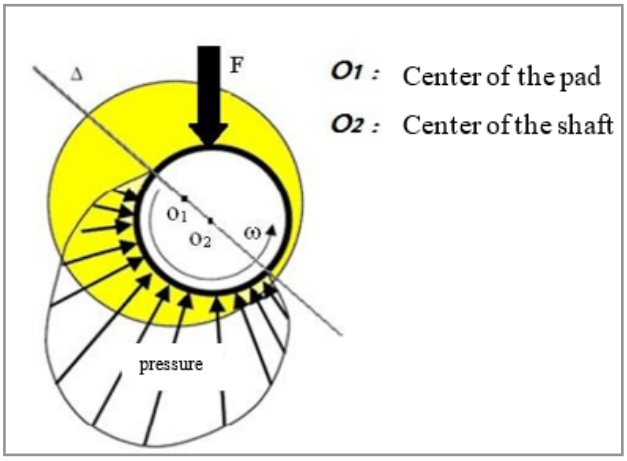

Figure 3: Hydrodynamic bearing with hydrodynamic pressure fields.

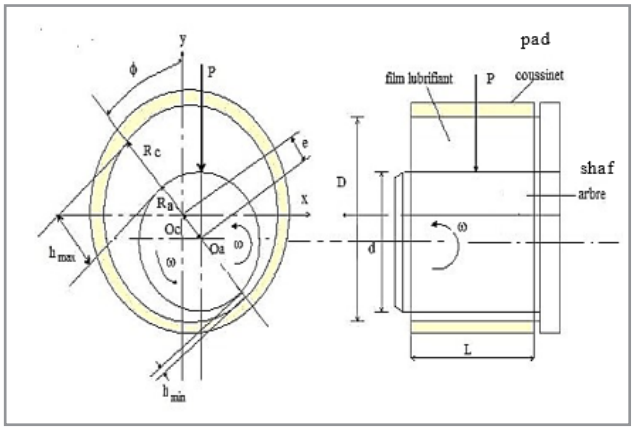

Figure 4: Hydrodynamic bearing operating characteristics.

In this case, a viscous fluid completely separates the surfaces present. The pressure in the film is created by the relative displacement of the surfaces and the geometry of the contact. HD bearings are fluid elements used to guide the shaft lines of rotating machines. These bearings fall into two categories: radial bearings and axial bearings also called thrust bearings.

Hydrodynamic Plain Bearings

This type of bearing is designed to operate in severe conditions (high loads and rotation frequencies). Therefore, to perform their function in perfect conditions, hydrodynamic bearings must be carefully designed.

There are two types of hydrodynamic bearing configuration:

- Fixed geometry bearings.
- Variable geometry bearings.

Basic Equations

The basic equations of the hydrodynamic bearing are used to study hydrodynamic contacts, assuming that the opposing surfaces are separated by a very thin, continuous fluid film with non- Newtonian behavior. These assumptions allow the fundamental laws of continuum mechanics to be used to describe the flow of the lubricating fluid in the contacts.

Hydrodynamic lubrication is an important field of tribology; it is the study of contacts in which a fluid film separates the surfaces involved. In the case where the fluid film completely separates the surfaces, the asperities and shape defects have dimensions smaller than the thickness of the film. The formation and maintenance of a fluid film requires the existence of pressure in this film in order to balance the load applied between the two surfaces of the mechanism.

Calculating this pressure allows us to determine the load that the contact can support, the friction torque and the flow rate of the mechanism. Thus, to determine the operating characteristics of a bearing, it will first be necessary to calculate the pressure in the film, the latter is obtained only by solving the Reynolds equation, which requires establishing some hypotheses and defining the boundary conditions concerning pressure and temperature.

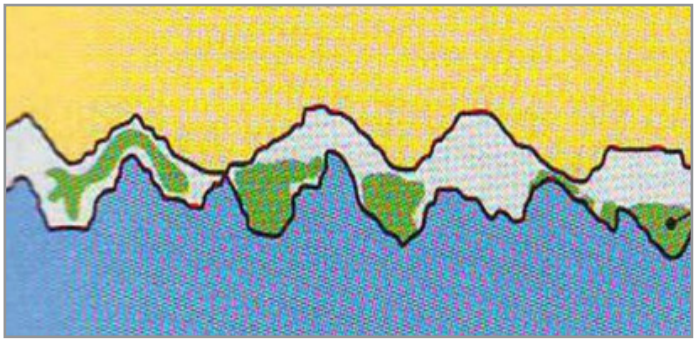

Figure 5: Schematic of a rough contact

To theoretically determine the characteristics of a lubricated contact such as plain bearings operating in a hydrodynamic lubrication regime, one must solve: the classical Reynolds equation in the case of a Newtonian fluid; the modified Reynolds equation for a non-Newtonian fluid (polar).

Reynolds Equation

The Reynolds equation is derived from the equations of continuum mechanics and the constitutive law of Newtonian fluids. We have the following equations:

The law of conservation of mass

$$\frac{\partial \rho}{\partial t} + \frac{\partial}{\partial x_i}(\rho u_i) = 0 \qquad i = 1.3 \tag{1}$$

The law of rheological behavior

Which for a Newtonian fluid is written:

$$T_{ij} = (-p + \lambda\theta)\delta_{ij} + 2\mu\varepsilon_{ij} \qquad i=1.3 \text{ and } j=1.3 \tag{2}$$

Tij : Component of the Cauchy stress tensor (Pa) or N/m²

P: Thermodynamic pressure (Pa) or N/m²

λ: Second coefficient of viscosity (Pa·s)

θ: Volumetric strain rate or divergence of velocity (s-1)

$$\theta = \frac{\partial u_1}{\partial x_1} + \frac{\partial u_2}{\partial x_2} + \frac{\partial u_3}{\partial x_3} \tag{3}$$

δij : Kronecker delta

μ : Dynamic viscosity (Pa·s)

j : Strain rate tensor (or rate of deformation tensor) (s-1)

$$\varepsilon_{ij} = \frac{1}{2}\left[\frac{\partial u_i}{\partial x_j} + \frac{\partial u_j}{\partial x_j}\right] \tag{4}$$

The law of conservation of momentum

$$\rho\left[\frac{\partial u_i}{\partial t} + u_j \frac{\partial u_i}{\partial x_j}\right] = \rho f_i + \frac{\partial \sigma_{ij}}{\partial x_j} \tag{5}$$

Thin Film Hypotheses

The Reynolds Equation is obtained by adopting the following thin film assumptions:

- The medium is continuous:The Reynolds equation is not valid in regions where the film breaks (e.g., due to cavitation).
- The film thickness is very small compared to the other contact dimensions.
- The fluid is Newtonian: There is a linear relationship between shear stress and shear rate within the film.
- One of the contact surfaces is perfectly flat and smooth:This allows placing the origin of the coordinate system on that surface. As a result, the general curvature of the film is neglected.

Form of the Equation

The Reynolds equation expresses the law of conservation of flow in contact. Depending on the axis system, it takes different forms.

- on wall 1, for y = 0: u = U1; v = 0; w = W1

- on wall 2, for y = h: u = U2; v = V2; w = W2

In these equations u,v and w represent the components of the fluid velocity in the X,Y and Z directions, respectively.

U_1 , U_2 , V_2 , W_1 et W_2 are the velocity components of surfaces 1 and 2 in the directions X,Y and Z.

The velocity V_1 of surface 1 in the Y direction is equal to zero. In this case, the fluid is governed by the following Reynolds equation.

$$\frac{\partial}{\partial x}\left[\frac{\rho h^3}{\mu}\frac{\partial p}{\partial x}\right]+\frac{\partial}{\partial z}\left[\frac{\rho h^3}{\mu}\frac{\partial p}{\partial z}\right]=6\rho(u_1-u_2)\frac{\partial h}{\partial x}+ 6\rho(w_1-w_2)\frac{\partial h}{\partial z}+6h\frac{\partial}{\partial x}[\rho(u_2+u_1)]+ 6h\frac{\partial}{\partial z}[\rho(w_2+w_1)]+12\rho v_2+12h\frac{\partial p}{\partial t} \quad (6)$$

To this Reynolds equation are added the equations giving the fluid velocities u and w in the X and Z directions, respectively:

$$\begin{cases} U=\frac{1}{2\mu}\frac{\partial p}{\partial x}y(y-h)+\frac{h-y}{h}u_1+\frac{y}{h}u_2 & (7)\\ w=\frac{1}{2\mu}\frac{\partial p}{\partial z}y(y-h)+\frac{h-y}{h}w_1+\frac{y}{h}w_2 & (8)\end{cases}$$

These relations allow us to determine the shear stresses in the fluid:

$$\begin{cases} \tau_{xy}=\mu\frac{\partial u}{\partial y}=\frac{1}{2}\frac{\partial p}{\partial x}(2y-h)+(u_2-u_1)\frac{\mu}{h} & (9)\\ \tau_{yz}=\mu\frac{\partial w}{\partial y}=\frac{1}{2}\frac{\partial p}{\partial z}(2y-h)+(w_2-w_1)\frac{\mu}{h} & (10)\end{cases}$$

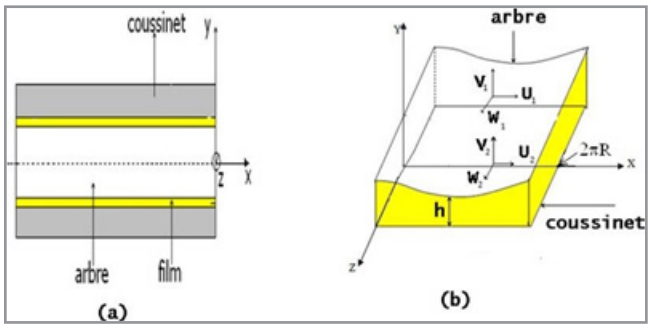

Figure 6: Bearing (a) and developed film (b)

Reynolds Equation of the Lubricated Bearing

The Reynolds equation is quite general; it applies to different types of contact and various lubricants. We can distinguish:

- Variable-viscosity and constant-viscosity fluids: it should be noted that for a variable-viscosity fluid, the viscosity does not vary across the film thickness.
- Compressible and incompressible fluids: in the latter case, the density disappears from the Reynold equation.
- Transient and steady-state regimes: in the mechanics of thin viscous films, the steady-state regime is defined as a regime in which, in a given reference frame (whether fixed or moving), the wall velocities and geometric parameters of the contact are time-independent.
- Hydrodynamic and hydrostatic contact: since the terminology is somewhat imprecise, we shall agree to define hydrostatic contact as the type of contact for which the Reynolds equation reduces to:

$$\frac{\partial}{\partial x}\left[\frac{\rho h^3}{\mu}\frac{\partial p}{\partial x}\right]+\frac{\partial}{\partial z}\left[\frac{\rho h^3}{\mu}\frac{\partial p}{\partial z}\right]=0 \text{ (Cartesian coordinates)} \quad (11)$$

It should be noted that these partial differential equations admit a non-trivial solution if and only if the pressure p is not zero at all points on the boundary of the integration domain, which proves the existence of an external pressure source outside the contact area.

The kinematic conditions related to the surfaces of the shaft and the bearing are expressed as:

$U_1=R_c\omega_c$

$V_1=w_1=0$

$U_2=R_a\omega_a\cos\alpha$

$V_2=R_a\omega_a\sin\alpha$

W=0

α: The angle between OcM' and OaM' is the slope of the curve h(x).

$$\tan\alpha=\frac{dh}{dx}=\frac{1}{R_a}\frac{dh}{d\theta}=-\frac{e}{R_a}\sin\theta \quad (12)$$

Since the quantity $\frac{e}{R_a}$ is very small, we can expand and limit ourselves to the 1st Order.

If we report the speeds of the contact surfaces in the Reynolds equation, written in Cartesian coordinates, and if we set R=R_a

$$\frac{\partial}{\partial x}\left[h^3\frac{\partial p}{\partial x}\right]+\frac{\partial}{\partial z}\left[h^3\frac{\partial p}{\partial z}\right]=6\mu R\,\omega\frac{\partial h}{\partial x} \quad (13)$$

This is the Reynolds Equation for our Roblem

Note:

- The bearing was developed and chosen as the reference plane; an identical result would have been obtained by developing the shaft.
- The angular velocities ωc and ωa, thus adding together, the lift is proportional to the sum of the velocities. If these are equal and opposite, the flow lift is zero to the second order.

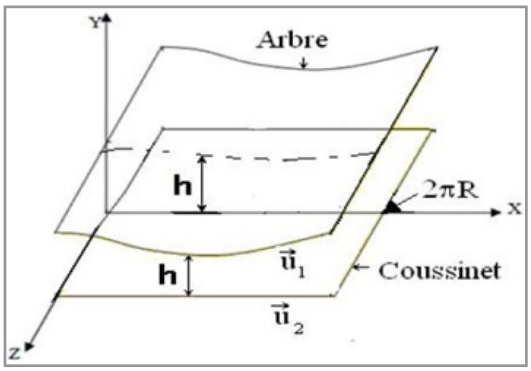

Figure 7: Developed Plain Bearing

Hydrodynamic Load and Pitch Angle

By integrating the pressure field, we obtain the components of the load on two perpendicular axes figure, they are written:

$$F_x = \int_S P\cos\theta ds = P\cos\varphi \quad (14)$$

$$F_y = \int_S P\sin\theta ds = P\sin\varphi \quad (15)$$

With:

$$P = \sqrt{f_x^2 + f_y^2} \quad (16)$$

The wedge angle is defined by:

$$\varphi = \text{arctg}\varphi = -(f_y / f_x) \quad (17)$$

The charge can be written as:

$$F_h = \int_0^L \int_0^{2\pi R} p\, dx\, dz \quad (18)$$

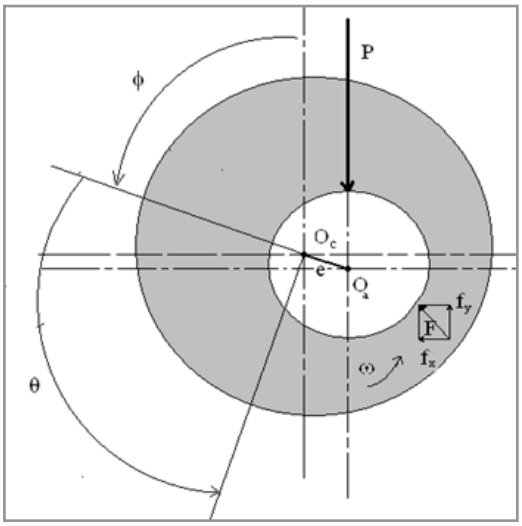

Figure 8: The Components of the Load

Fundamental Laws of Continuum Mechanics for a non-Newtonian Fluid (Polar Fluid)

According to the theory of Vijay Kumar Stokes [24], the basic equations for writing the motion of non-Newtonian fluids called Couple Stress fluids or polar fluids in the case where the volume forces and volume couples are negligible, are the law of conservation of mass (1), the law of conservation of momentum (5), to which we add a third equation which is written:

$$\frac{\partial M_{ji}}{\partial x_i} + e_{ijk}\,\sigma_{jk} = 0 \quad (19)$$

For this type of fluid, the rheological behavior law takes the following form:

$$\sigma_{ij} = -p\,\delta_{ij} + 2\,\mu\varepsilon_{ij} - \frac{1}{2} e_{ijk} \frac{\partial M_{rk}}{\partial x_r} \quad (20)$$

With:

$$M_{rk} = \frac{1}{3} M_{ij}\,\delta_{rk} + 4\eta \frac{\partial w_k}{\partial x_r} + 4\eta' \frac{\partial w_r}{\partial x_k} \quad (21)$$

$$\omega_i = \frac{1}{2} e_{ijk} \frac{\partial u_k}{\partial x_j} \quad \text{ou} \quad \vec{\omega} = \frac{1}{2} \overrightarrow{rot}\, \vec{V} \quad (22)$$

e_{ijk} : is the permutation tensor

M_{ij} : the tensor of the stress couples in the fluid

η and η′ : are the physical constants responsible for the stress couple in the fluid

ωi : the components of the rotation vector or the vorticity vector $\vec{\omega}$

Equations of Motion

* Navier-Stokes equations

Based on the theory of continuous micro-media by V. K. Stokes [47], the equations of motion for an incompressible fluid with stress couples are written by taking into account body forces and body couples:

$$\rho \frac{D\vec{V}}{Dt} = -\vec{\nabla}p + \rho\vec{B} + \frac{1}{2}\vec{\nabla} \times (\rho\vec{C}) + \mu\,\vec{\nabla}^2\vec{V} - \eta\,\vec{\nabla}^4\vec{V} \quad (23)$$

Where the vectors V,B and C represent respectively the velocity field, the force per unit mass and the volume torque per unit mass.

Neglecting volume forces and torques, equation (19) reduces to:

$$\rho\left(u_j \frac{\partial u_1}{\partial x_j}\right) = -\frac{\partial p}{\partial x_1} + \mu\left(\frac{\partial^2 u_1}{\partial x_1^2} + \frac{\partial^2 u_1}{\partial x_2^2} + \frac{\partial^2 u_1}{\partial x_3^2}\right) - \eta\left(\frac{\partial^4 u_1}{\partial x_1^4} + \frac{\partial^4 u_1}{\partial x_2^4} + \frac{\partial^4 u_1}{\partial x_3^4}\right) - 2\eta\left(\frac{\partial^4 u_1}{\partial x_1^2 \partial x_2^2} + \frac{\partial^4 u_1}{\partial x_1^2 \partial x_3^2} + \frac{\partial^4 u_1}{\partial x_2^2 \partial x_3^2}\right) \quad (24)$$

$$\rho\left(u_j \frac{\partial u_2}{\partial x_j}\right) = -\frac{\partial p}{\partial x_2} + \mu\left(\frac{\partial^2 u_2}{\partial x_1^2} + \frac{\partial^2 u_2}{\partial x_2^2} + \frac{\partial^2 u_2}{\partial x_3^2}\right) - \eta\left(\frac{\partial^4 u_2}{\partial x_1^4} + \frac{\partial^4 u_2}{\partial x_2^4} + \frac{\partial^4 u_2}{\partial x_3^4}\right) - 2\eta\left(\frac{\partial^4 u_2}{\partial x_1^2 \partial x_2^2} + \frac{\partial^4 u_2}{\partial x_1^2 \partial x_3^2} + \frac{\partial^4 u_2}{\partial x_2^2 \partial x_3^2}\right) \quad (25)$$

$$\rho\left(u_j \frac{\partial u_3}{\partial x_j}\right) = -\frac{\partial p}{\partial x_3} + \mu\left(\frac{\partial^2 u_3}{\partial x_1^2} + \frac{\partial^2 u_3}{\partial x_2^2} + \frac{\partial^2 u_3}{\partial x_3^2}\right) - \eta\left(\frac{\partial^4 u_3}{\partial x_1^4} + \frac{\partial^4 u_3}{\partial x_2^4} + \frac{\partial^4 u_3}{\partial x_3^4}\right) - 2\eta\left(\frac{\partial^4 u_3}{\partial x_1^2 \partial x_2^2} + \frac{\partial^4 u_3}{\partial x_1^2 \partial x_3^2} + \frac{\partial^4 u_3}{\partial x_2^2 \partial x_3^2}\right) \quad (26)$$

J=1, 2, 3

Equations of Motion for Thin Film Flow

To determine the order of magnitude of the different terms of equations (20), we use the same reduced variables as in the previous case to which we add $\tilde{\eta} = \frac{\eta}{\eta_0}$ and $l_0 = \sqrt{\frac{\eta_0}{\mu_0}}$ Taking into account these changes of variable, equations (20) are written:

$$\frac{\partial \tilde{p}}{\partial \tilde{x}_1} = -\varepsilon\, \tilde{\rho}\, R_h\, \tilde{u}_j \frac{\partial \tilde{u}_1}{\partial \tilde{x}_j} + \tilde{\mu}\left[\varepsilon^2 \frac{\partial^2 \tilde{u}_1}{\partial \tilde{x}_1{}^2} + \frac{\partial^2 \tilde{u}_1}{\partial \tilde{x}_2{}^2} + \varepsilon^2 \frac{\partial^2 \tilde{u}_1}{\partial \tilde{x}_3{}^2} \right] - \tilde{\eta} \left(\frac{l_0}{h}\right)^2 \left(\varepsilon^4 \frac{\partial^4 \tilde{u}_1}{\partial \tilde{x}_1{}^4} + \frac{\partial^4 \tilde{u}_1}{\partial \tilde{x}_2{}^4} + \varepsilon^4 \frac{\partial^4 \tilde{u}_1}{\partial \tilde{x}_3{}^4} \right) - 2\, \tilde{\eta} \left(\frac{l_0}{h}\right)^2 \varepsilon^2 \left[\frac{\partial^4 \tilde{u}_1}{\partial \tilde{x}_1{}^2 \partial \tilde{x}_2{}^2} + \varepsilon^2 \frac{\partial^4 \tilde{u}_1}{\partial \tilde{x}_1{}^2 \partial \tilde{x}_3{}^2} + \frac{\partial^4 \tilde{u}_1}{\partial \tilde{x}_2{}^2 \partial \tilde{x}_3{}^2} \right] \quad (27)$$

$$\frac{\partial \tilde{p}}{\partial \tilde{x}_2} = \varepsilon^2 \left[-\varepsilon \tilde{\rho} R_h\, \tilde{u}_j \frac{\partial \tilde{u}_2}{\partial \tilde{x}_j} + \tilde{\mu} \left[\varepsilon^2 \frac{\partial^2 \tilde{u}_2}{\partial \tilde{x}_1{}^2} + \frac{\partial^2 \tilde{u}_2}{\partial \tilde{x}_2{}^2} + \varepsilon^2 \frac{\partial^2 \tilde{u}_2}{\partial \tilde{x}_3{}^2} \right] - \tilde{\eta} \left(\frac{l_0}{h}\right)^2 \left[\varepsilon^4 \frac{\partial^4 \tilde{u}_2}{\partial \tilde{x}_1{}^4} + \frac{\partial^4 \tilde{u}_2}{\partial \tilde{x}_2{}^4} + \varepsilon^4 \frac{\partial^4 \tilde{u}_2}{\partial \tilde{x}_3{}^4} \right] - 2\, \tilde{\eta} \left(\frac{l_0}{h}\right)^2 \varepsilon^2 \left[\frac{\partial^4 \tilde{u}_2}{\partial \tilde{x}_1{}^2 \partial \tilde{x}_2{}^2} + \varepsilon^2 \frac{\partial^4 \tilde{u}_2}{\partial \tilde{x}_1{}^2 \partial \tilde{x}_3{}^2} + \frac{\partial^4 \tilde{u}_2}{\partial \tilde{x}_2{}^2 \partial \tilde{x}_3{}^2} \right] \right] \quad (28)$$

$$\frac{\partial \tilde{p}}{\partial \tilde{x}_3} = -\varepsilon\, \tilde{\rho}\, R_h\, \tilde{u}_j \frac{\partial \tilde{u}_3}{\partial \tilde{x}_j} + \tilde{\mu}\left[\varepsilon^2 \frac{\partial^2 \tilde{u}_3}{\partial \tilde{x}_1{}^2} + \frac{\partial^2 \tilde{u}_3}{\partial \tilde{x}_2{}^2} + \varepsilon^2 \frac{\partial^2 \tilde{u}_3}{\partial \tilde{x}_3{}^2} \right] - \tilde{\eta} \left(\frac{l_0}{h}\right)^2 \left(\varepsilon^4 \frac{\partial^4 \tilde{u}_3}{\partial \tilde{x}_1{}^4} + \frac{\partial^4 \tilde{u}_3}{\partial \tilde{x}_2{}^4} + \varepsilon^4 \frac{\partial^4 \tilde{u}_3}{\partial \tilde{x}_3{}^4} \right) - 2\, \tilde{\eta} \left(\frac{l_0}{h}\right)^2 \varepsilon^2 \left[\frac{\partial^4 \tilde{u}_3}{\partial \tilde{x}_1{}^2 \partial \tilde{x}_2{}^2} + \varepsilon^2 \frac{\partial^4 \tilde{u}_3}{\partial \tilde{x}_1{}^2 \partial \tilde{x}_3{}^2} + \frac{\partial^4 \tilde{u}_3}{\partial \tilde{x}_2{}^2 \partial \tilde{x}_3{}^2} \right] \quad (29)$$

Neglecting the terms multiplied by ε^2 and ε^4, it remains:

$$\frac{\partial \tilde{p}}{\partial \tilde{x}_i} = -\varepsilon\, \tilde{\rho}\, R_h\, \tilde{u}_j \frac{\partial \tilde{u}_i}{\partial \tilde{x}_j} + \tilde{\mu} \frac{\partial^2 \tilde{u}_i}{\partial \tilde{x}_2{}^2} - \tilde{\eta} \left(\frac{l_0}{h}\right)^2 \frac{\partial^4 \tilde{u}_3}{\partial \tilde{x}_2{}^4}$$

i=1 et 3 (30)

$$\frac{\partial \tilde{p}}{\partial \tilde{x}_2} = 0 \longrightarrow \tilde{p} = \tilde{p}\,(\tilde{x}_1, \tilde{x}_3) \quad (31)$$

If the inertial forces are negligible, it comes:

$$\frac{\partial p}{\partial x_i} = \mu \frac{\partial^2 u_i}{\partial x_2{}^2} - \eta \frac{\partial^4 u_i}{\partial x_2{}^4} \quad (32)$$

$$\frac{\partial p}{\partial x_2} = 0 \quad (33)$$

To highlight the dominant terms, it is convenient to rewrite the equations for the incompressible fluid in dimensionless form. The change of variables adopted is as follows:

- Space and time variables

$$\tilde{x}_1 = \frac{x_1}{L},\ \tilde{x}_2 = \frac{x_2}{L},\ \tilde{x}_3 = \frac{x_3}{h},\ \tilde{t} = t\frac{V}{L} \quad (34)$$

- Components of flow velocity

$$\tilde{u}_1 = \frac{u_1}{V},\ \tilde{u}_2 = \frac{u_2}{V},\ \tilde{u}_3 = u_3 \frac{L}{Vh} \quad (35)$$

- Physical constants of the fluid

$$\tilde{\rho} = \frac{\rho}{\rho_0},\quad \tilde{\mu} = \frac{\mu}{\mu_0} \quad (36)$$

This change leads us to ask

$$\tilde{p} = p \frac{h^2}{\mu_0 V L} \quad (37)$$

Or:

V is the speed of one of the contact walls.

L is the characteristic dimension of the contact.

μ0 ρ0 are respectively the dynamic viscosity and the reference density at T=T0

Modified Reynolds equation

The components of the flow vector per unit length along x1 and x3 for a non-Newtonian fluid are written

$$\begin{cases} q_1 = -\frac{G(h,l)}{12\mu} \frac{\partial p}{\partial x_1} + \frac{h}{2}(u_{11} + u_{21}) \\ q_3 = -\frac{G(h,l)}{12\mu} \frac{\partial p}{\partial x_3} + \frac{h}{2}(u_{13} + u_{23}) \end{cases} \quad (38)$$

$$G(h,l) = h^3 - 12\, l^2 h + 24\, l^3\, th\left(\frac{h}{2l}\right) \quad (39)$$

Then the modified Reynolds equation is written as

$$\frac{\partial}{\partial x_1}\left(\frac{G(h,l)}{12\mu} \frac{\partial p}{\partial x_1} \right) + \frac{\partial}{\partial x_3}\left(\frac{G(h,l)}{12\mu} \frac{\partial p}{\partial x_3} \right) = \frac{\partial p}{\partial x_1}\left(\frac{h}{2}(u_{11} + u_{21}) \right) + \frac{\partial p}{\partial x_3}\left(\frac{h}{2}(u_{13} + u_{23}) \right) + \frac{\partial h}{\partial t} \quad (40)$$

Digital Simulation

This study aims to better predict the non- Newtonian behavior of the oil film in bearings operating under more severe conditions. The rotation speed varies from 1000 to 9000 tr/min and the radial load varies from 2 to 10 kN. The temperature and pressure within the supposedly non-Newtonian fluid film are high, with a coefficient n greater than 1 that is to say for viscoelastic fluids.

The Digital Resolution Strategy

The digital resolution strategy for an ANSYS CFX code is:

- Modeling of the structure.
- Mesh.
- Load modeling.
- Resolution of the Navier stocks equation by the finite volume method.
- Calculation of the operating characteristics of the bearing.

Overview of the problem

The simulation is carried out for a hydrodynamic plain bearing of finite dimensions. The diameter of the bearing is 100mm and the length is 80mm, the diameter of the shaft is 99.98. The main geometric characteristics as well as the characteristics of the lubricant are reported in table 5.1.

Table 1: Geometric characteristics of the bearing and lubricant characteristics

parameter	value
Bearing diameter (mm)	100
Shaft diameter (mm)	99.91
Bearing length (mm)	70
Radial clearance (mm)	0.09
Pad thickness (mm)	4
Feed port diameter (mm)	14
Groove length (mm)	70
Starting speed (tr/min)	1000-9000
Radial load (N)	2000-10,000
Supply temperature Ta (°C)	60
Supply pressure Pa (MPa)	0.04
Type of lubricant	PMA 3
Density (Kg/m3)	800
Specific heat (J/Kg.K)	2000
Kinematic viscosity (mm^2/s)	17.49
Rotation speed (rpm)	1000-9000
Radial load (N)	2-10
Ambient temperature (°C)	60

The geometry is made using ICEM CFD, figure 5 illustrates the geometry of the bearing studied while respecting its dimensions. The geometry was discretized with a mixed structured mesh; the shaft and the bearing were divided into 20 nodes following the circumference, 103 nodes following the length.

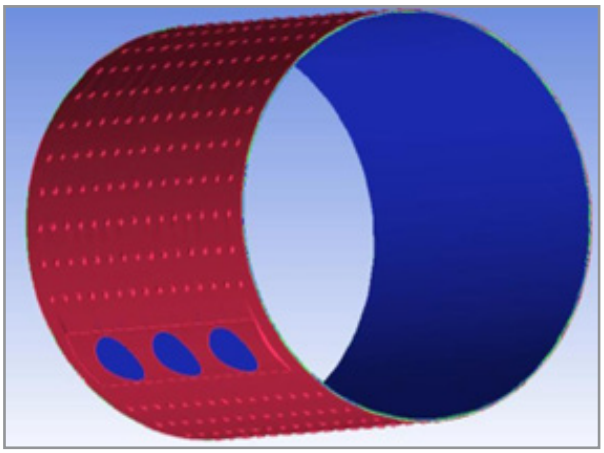

Figure 9: Geometry of the bearing.

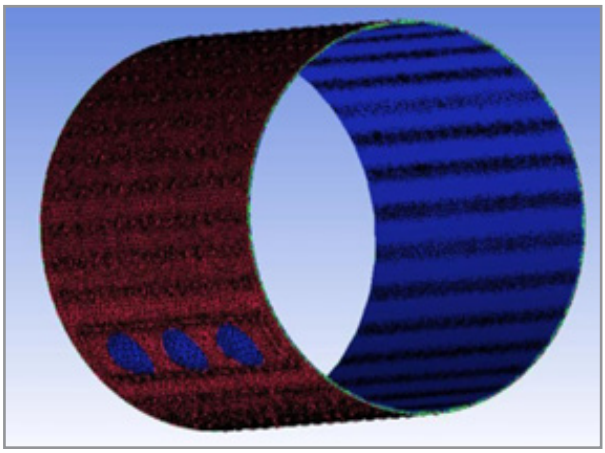

Figure 10: Mesh presentation of the textured surface bearing.

Results and Discussion

Behavior of a non-Newtonian fluid in a hydrodynamic plain bearing with a textured and non-textured surface

1.2.1 Influence of the speed of rotation, radial load W = 2000 N and n = 1.25, n = 1.5

Figures 11 and 12 illustrate the variation of pressure in non-textured and textured plain bearings as a function of rotational speed, under a radial load of 2000 N. The lubricant is modeled as a non-Newtonian fluid following the Ostwald–de Wale power-law model with flow behavior indices n=1.25 and n=1.5.

In Figure 11, the pressure distribution for n=1.25 shows a clear dependence on the rotational speed. The pressure magnitude decreases progressively with increasing speed, indicating the sensitivity of the hydrodynamic film to shear rate variations.

Figure 12 presents the circumferential pressure variation for the same load conditions. The most significant pressure values are observed at the lowest rotational speed (1000 rpm). For the untextured bearing, the pressure decreases by approximately 22% when the speed increases from 1000 to 9000 rpm for n=1.25, and by about 42% for n=1.5. A pronounced oil film rupture zone appears between angular positions 200° and 250° for the bearing operating at 9000 rpm under a 2000 N radial load, confirming the weakening of the hydrodynamic film at higher speeds.

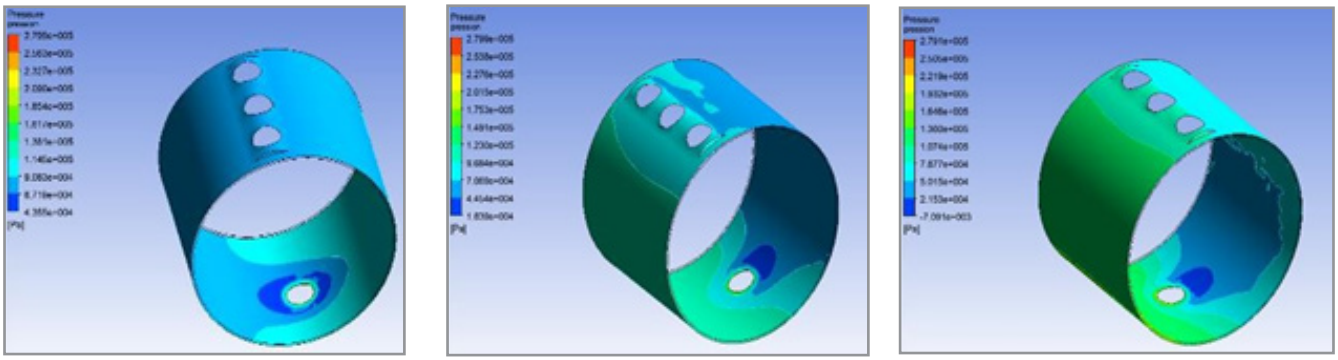

1000 rpm 5000 rpm 9000 rpm

Figure 11a: Pressure distribution in Non-textured bearing of the 3D View

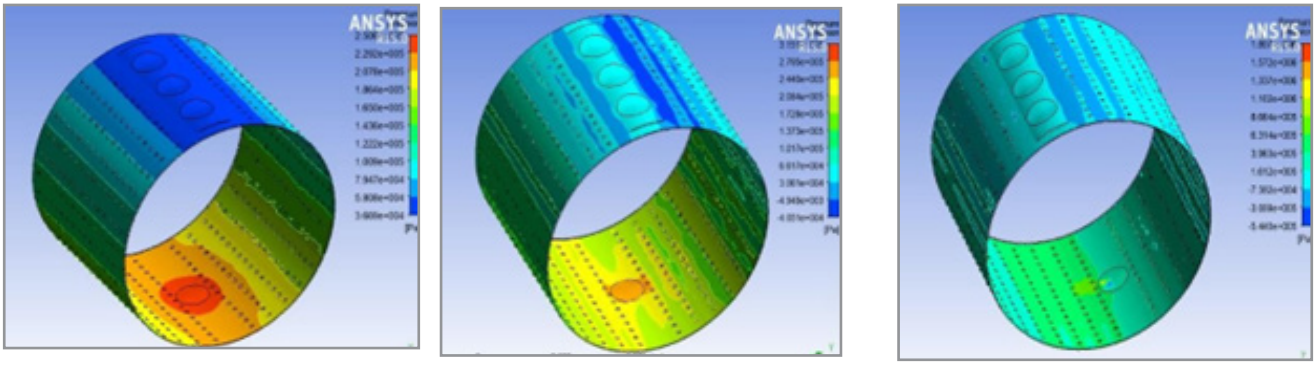

1000 rpm 5000 rpm 9000 rpm

Figure 11b: Pressure distribution in textured plain bearing of the 3D View

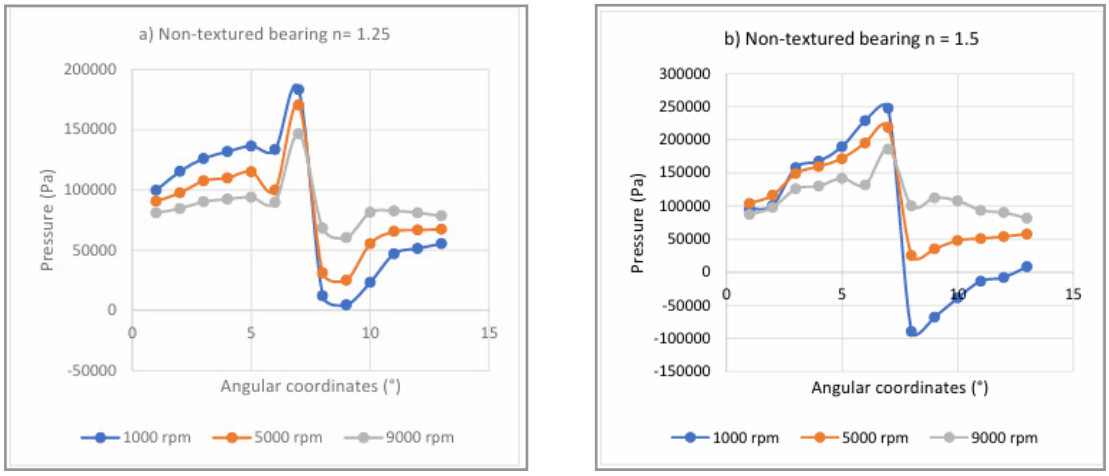

Figure 12: Pressure distribution according to the circumference of the plain bearing for different rotational speeds (power law n = 1.25 et n = 1.5)

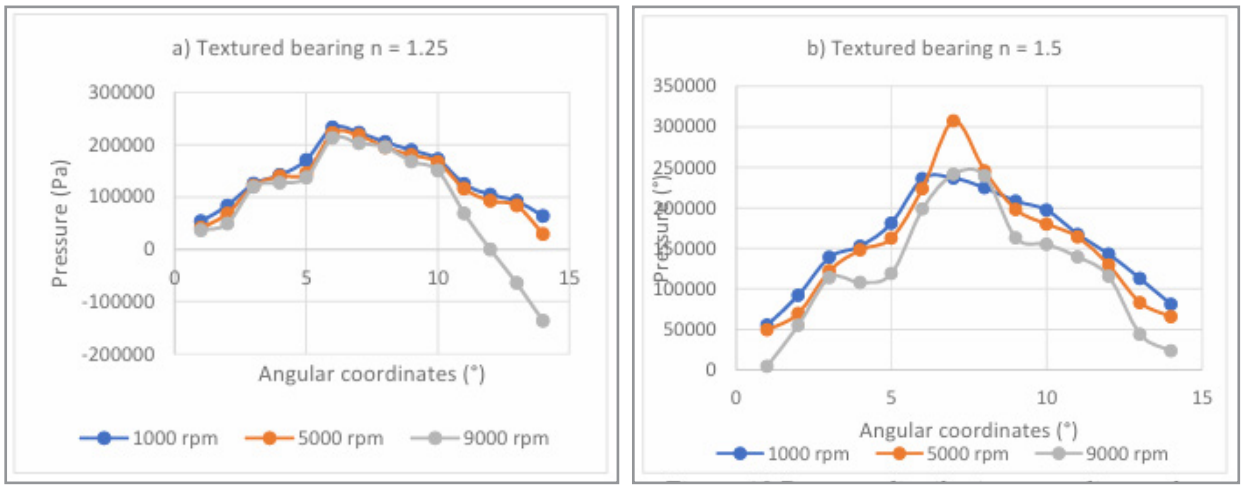

Figure 13: Pressure distribution according to the circumference of the textured plain bearing for different rotational speeds (power law n = 1.25 et n= 1.5)

Figure 13 illustrates the pressure distribution along the median plane of a cylindrical plain bearing with a textured surface, for rotational speeds ranging from 1000 to 9000 rpm under a radial load of 2000
N. The analysis was carried out using the Ostwald– de Waele power-law model with flow behavior indices n=1.25 and n=1.5. The results show that the pressure decreases with increasing rotational speed, with maximum values observed between angular coordinates 170° and 190°. In the textured configuration, the pressure reduction due to speed variation is approximately 9% for n=1.25 and 15% for n=1.5. Influence of the Radial Load (N = 9000 rpm, n = 1.25 and n = 1.5).

To evaluate the influence of the radial load on the hydrodynamic performance of plain bearings with textured and untextured surfaces, a parametric analysis was performed for three load conditions: W1=2000 N, W2=6000 N, and W3=10,000 N. The operating parameters were fixed as follows: supply temperature Ta=60∘C, supply pressure Pa=0.04 MPa, and shaft rotational speed of 9000 rpm. The lubricant behavior was modeled using the Ostwald–de Wale power-law with n=1.25 and n=1.5.

Figure 14 presents the evolution of pressure along the median plane for both textured and untextured plain bearings under the three load conditions, with n=1.25. The results show that pressure increases significantly with the applied radial load.
Figure 15 depicts the hydrodynamic pressure distribution for loads of 2000 N, 6000 N, and 10 000 N, confirming that the pressure rises with increasing load when considering non-Newtonian fluid behavior.

For the untextured bearing, the pressure increase reaches approximately 13% for n=1.25 and 46% for n=1.5. Conversely, for the textured bearing, the corresponding increases are 39% for n=1.25 and 67% for n=1.5, as shown in Figure 16. Moreover, a pronounced film rupture zone is observed under the highest load condition (10 000 N), indicating a degradation of the hydrodynamic film stability.

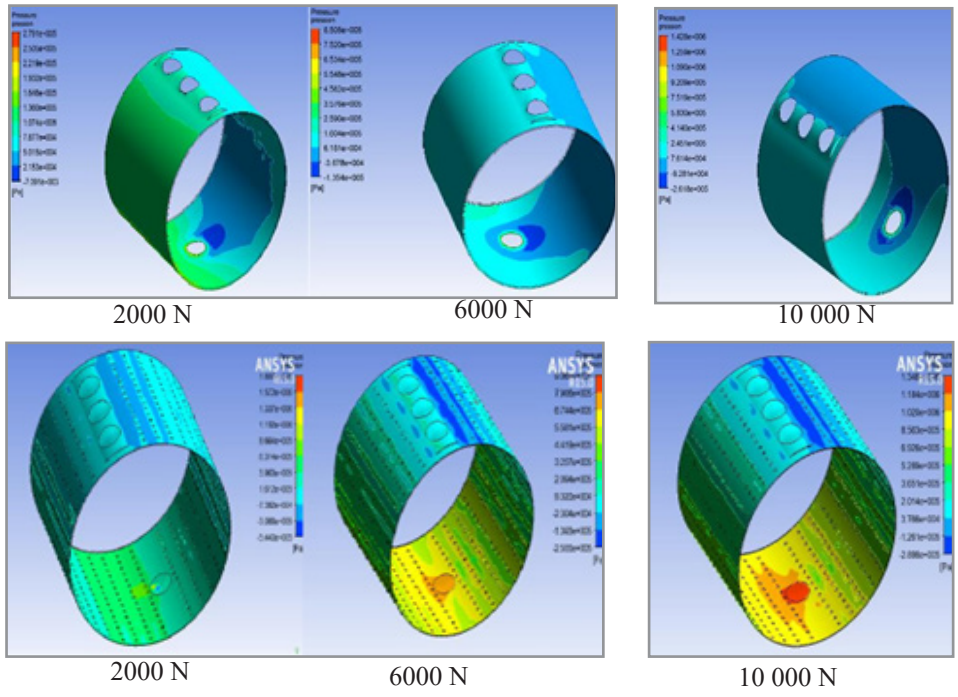

Figure 14: Circumferential pressure distribution

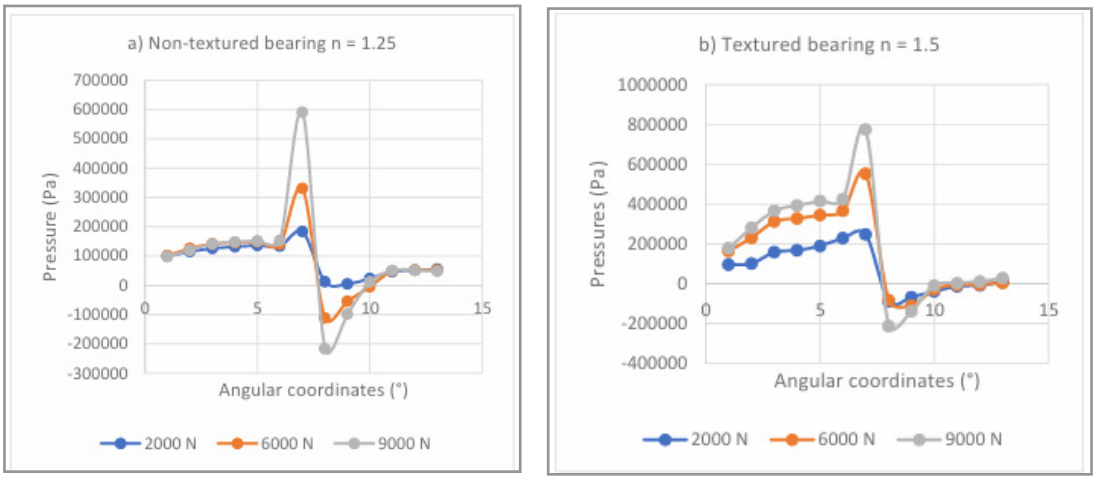

Figure 15: Variation of the circumferential pressure of a non-textured bearing for different radial loads (power law n = 1.25 et n= 1.5)

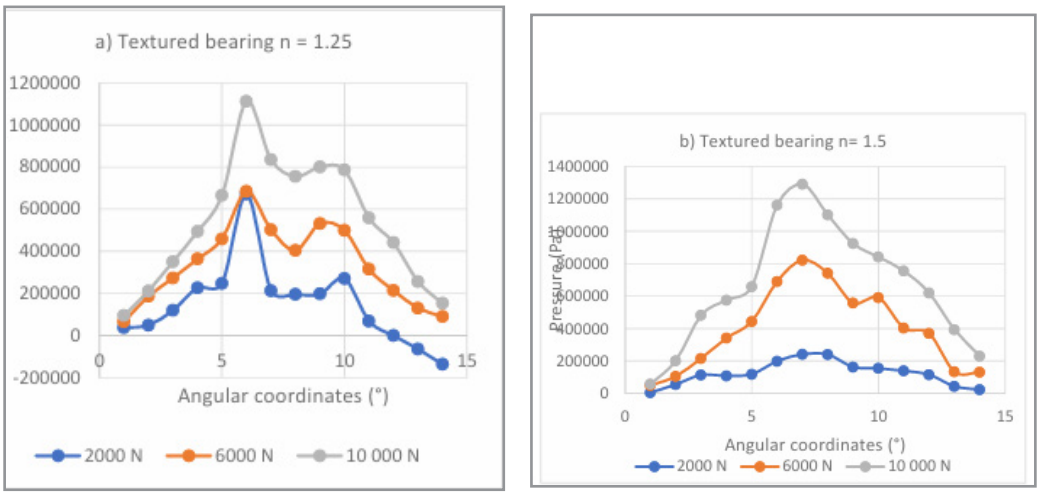

Figure 16: Pressure along the median plane of the textured bearing for different radial loads (Power Law n = 1.25 and n = 1.5) W = 2000 N and N = 9000 rpm

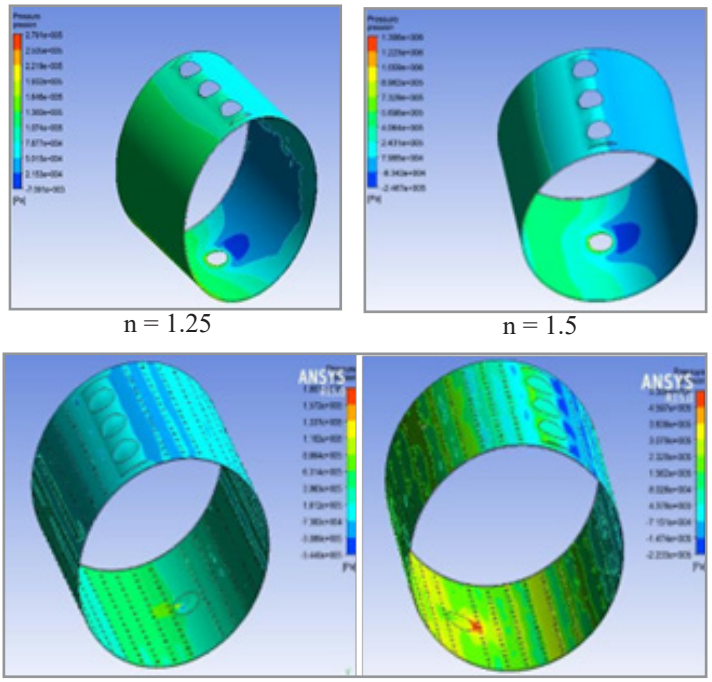

n = 1.25 n = 1.5

n = 1.25 n = 1.5

Figure 17: Pressure evolution of the untextured and textured plain bearing for n = 1.25 and n = 1.5

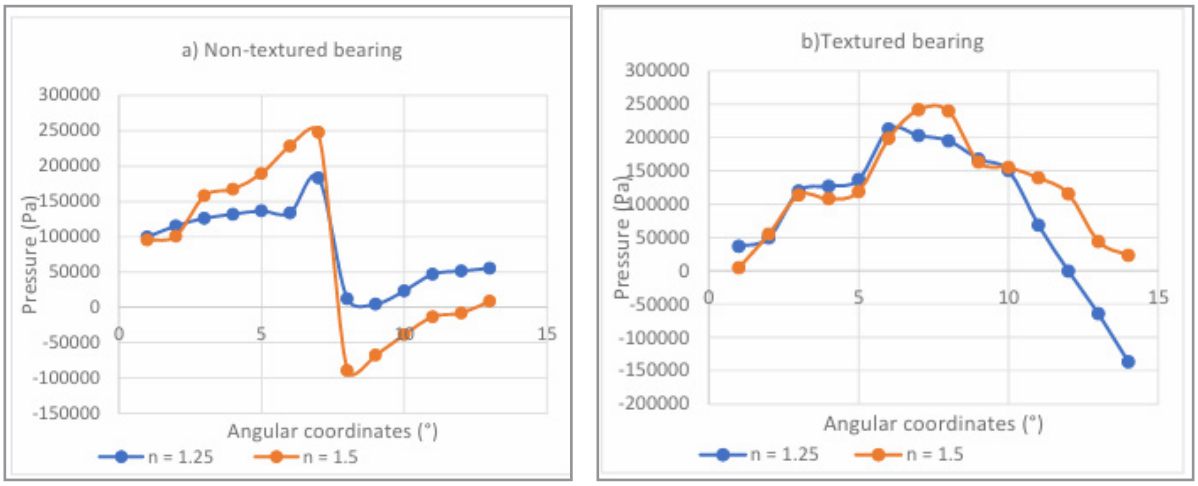

Figure 18: Pressure distribution as a function of the angular coordinate for both textured and untextured plain bearings at various power-law indices n.

Figures 17 and 18 present the pressure distribution along the mid-plane of both untextured and textured cylindrical plain bearings under a radial load of 2000 N and a rotational speed of 9000 rpm. The lubricant is modeled as a non-Newtonian fluid following the Ostwald–de Waele power-law model, with power-law indices n=1.25 and n=1.5. Although the general pressure distribution remains similar for both cases, higher pressure magnitudes are observed for n=1.5n = 1.5n=1.5.

Influence of the Power-Law Index n

The evolution of pressure with different power-law indices nnn is illustrated in Figures 19 and 20, corresponding to a radial load of 2000 N and a rotational speed of 9000 rpm. The maximum pressure occurs for n=1.5, indicating the behavior of a visco-plastic fluid. In contrast, for shear- thinning fluids characterized by n<1n < 1n<1 (i.e., n=0.5 and n=0.75), a rupture zone of the lubricant film appears, highlighting the reduced load- carrying capacity in these cases.

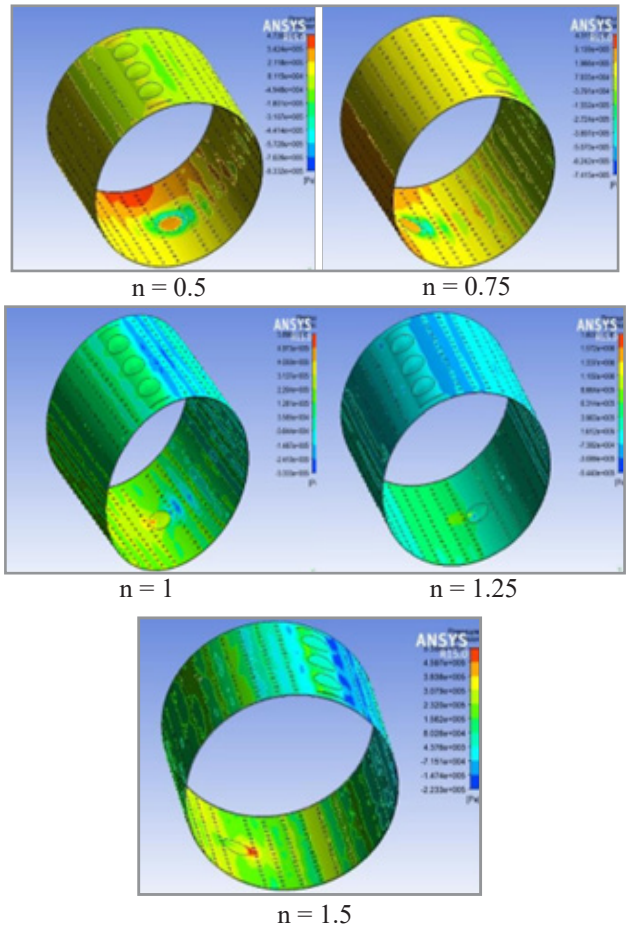

Figure 19: Three-dimensional distribution of hydrodynamic pressure in a plain bearing for different flow behavior indices nnn

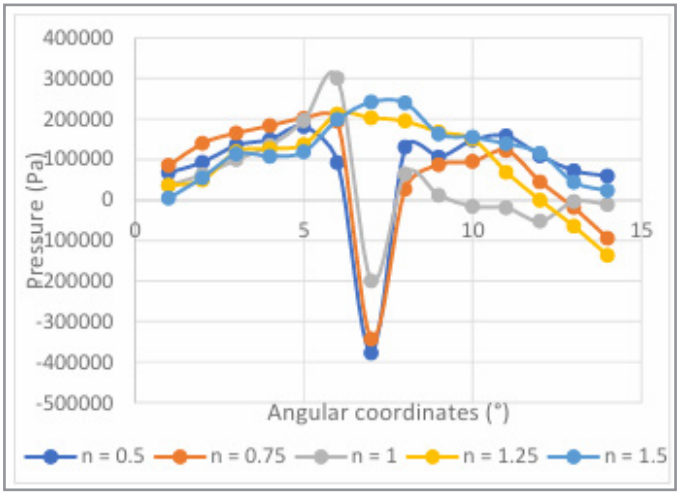

Figure 20: Pressure distribution versus angular position for a textured bearing under various power-law indices nnn.

Conclusion

A comprehensive numerical analysis was onducted to investigate the behavior of a non- Newtonian luid in a finite-length hydrodynamic plain bearing with both textured and untextured surfaces. The study employed a CFD omputational framework, ensuring high accuracy and robustness in odeling complex flow phenomena. The energy equation was solved using the finite difference method for various operating conditions, with rotational peeds ranging from 1000 to 9000 rpm and radial loads etween 2 and 10 kN. The numerical results were validated

against the data reported by Dr. Mehala in previous studies.

Key findings are summarized as follows:

- For both bearing configurations under a 2000 N radial load, the pressure distribution governed by the Ostwald–de Waele power- law model shows higher pressure near the supply ports.
- Increasing the rotational speed reduces the circumferential pressure between angular positions 150°–190° by approximately 22% for n=1.25n, while an increase is observed between 190°–335°. The maximum pressure occurs at 190° for the untextured bearing operating at 1000 rpm.
- Raising the flow behavior index nnn leads to a 42% decrease in pressure for n=1.5. A cavitation zone appears between 200° and 250° for the untextured bearing at 1000 rpm.
- In the textured configuration, the pressure decreases with increasing rotational speed (1000–9000 rpm), with maximum values at 170°–190°. The pressure reduction reaches 9% for n=1.25 and 15% for n=1.5.
- The circumferential pressure increases with higher radial loads. For an untextured bearing operating at 9000 rpm and 10 000 N, the pressure rise reaches 13% for n=1.25 and 46% for n=1.5. For the textured bearing, the corresponding increases are 39% and 67%.
- Under identical operating conditions (2000 N, 9000 rpm), the pressure magnitude is greater for n=1.5n = 1.5n=1.5 than for n=1.25n = 1.25n=1.25.
- Additionally, increasing the radial load enhances the lubricant film velocity, improving the hydrodynamic pressure buildup.

References

1. Gecim, B. A. (1990). Non-Newtonian effects of multi-grade oils on journal bearing performance. STLE Tribology Transactions, 33(3), 384-394.
2. Lemaître, F., Berker, A. (1995). Non-Newtonian cavitation analysis in journal bearings. Journal of Non-Newtonian Fluid Mechanics, 59(1), 31-48.
3. Zhang, C., Zhang, Z., Qiu, Z. (1998). Analysis of mixed lubrication of dynamically loaded journal bearings including non-Newtonian effects and mass conserving cavitation. In Proceedings of the 24th Leeds-Lyon Symposium on Tribology (pp. 175–186). September 1997.
4. Zhang, C. Cheng, H. S. (2002). Transient Non- Newtonian Thermohydrodynamic Mixed Lubrication of Dynamically Loaded Journal Bearings," ASME J. Tribology., 122, 156-161.
5. Wang,P. Keith, T. G. Vaidyanathan,K.(2001). Non- Newtonian Effects on the Performance of Dynamically Loaded Elliptical Journal Bearings Using a Mass-Conserving Finite Element Cavitation Algorithm", STLE Tribology Transaction, 44(4), 533-542.
6. Wang,P. Keith,T.G. Vaidyanathan,K.(2002). "Combined Surface Roughness Pattern and Non- Newtonian Effects on the Performance of Dynamically Loaded Journal Bearings", STLE Tribology Transaction, 45(1), 1-10.
7. Boucherit, H. (2002). Dynamic behavior of fluid bearings of rotating machines linear and nonlinear analysis, Master's thesis.
8. Fatu, A. (2005). Numerical and experimental modeling of the lubrication of motor bearings subjected to drying conditions, Thèse de Doctorat, doctoral school of sciences for the engineer of the University of Poitiers.
9. Frêne, J. Engineering techniques, article B5320- Hydrodynamic thrust bearings and bearings.
10. Javorova, J., Mazdrakova, A., Andonov, I., Radulescu, A. (2016). Analysis of HD Journal Bearings Considering Elastic Deformation and Non-Newtonian Rabinowitsch Fluid Model, Triboloby in Industry, vol. 38(2), 186-196, 2016.
11. Kamla, Y. (2011). Study of the flow of a non-Newtonian fluid in a tank mechanically agitated by a Rushton Turbine. Doctoral thesis, University of Science and Technology of Oran, Energy and environment, Thermal machines, applications and environmental risks.
12. Kane, M. (2003). The effect of roughness and non- Newtonian effects in severe lubricated contacts, Doctoral Thesis, National Institute of Applied Sciences of Lyon.

13. Kasai, M. (2010). Reducing friction and improving the reliability of the bearing lubrication with automotive engine oils. Doctoral thesis, University of Poitiers, specialty Mechanical Engineering, Industrial Engineering, Transportation.
14. Lahmar, M., Boucherit, H. (2006). Comparative study of the nonlinear dynamic behavior of a damping bearing and a fluid bearing.12
15. Mehala, K. (2015). Study of the evolution of the lubrication regime during the transient phase in hydrodynamic bearings, Doctoral thesis, University of Science and Technology of Oran (Mohammed Boudiaf).
16. Mehala, K. Bendaoud, N. Youcefi,A. (2016). Numerical Analyses of the Non-Newtonian Flow Performance and Thermal Effect on a Bearing Coated with a High Tin Content, Tribology in Industry, 38(4), 575-584.
17. Nouar, A. (2005). Analysis of stresses and deformations of tubes and cylindrical sectors: application to the resolution of fluid-structure interaction problems in hydrodynamic bearings. Master's thesis.
18. Sahli, A. (2011). Experimental study of a lubricated misaligned bearing, master's thesis, University of Hassiba Ben Bouali Chlef.
19. Zerrouni, N. (2009). Study of the viscous fluid- structure interaction of a fluid bearing subjected to temporal stresses, Magister thesis, University of M'hamed Bougara-Boumerdes.